Generalized Coupled Interconnect Transfer Function and High-Speed Signal Simulations

Yungseon Eo and William R. Eisenstadt

Abstract—**A new expression for the coupled interconnect system transfer function has been derived under general linear generator and uncoupled load conditions, i.e., without any restrictions in circuit load impedance. High-speed signals on coupled interconnects have been simulated using this transfer function. The simulation uses generalized interconnect circuit model parameters in which all line parameters are frequency dependent. The validity of the interconnect circuit parameters was confirmed previously using s-parameter measurements. High-speed signal simulation using this novel interconnect transfer function has been verified with time-domain measurements using an HP54121T high-speed sampling oscilloscope. This work accurately predicts coupled interconnect circuit responses. With this transfer function, signal integrity problems of high-performance VLSI circuits can be predicted in the design stage.**

I. Introduction

With the rapid increase of integration level and speed, IC interconnect becomes one of the important limiting factors of today's VLSI circuit design performance. The chip area occupied by interconnect, as well as the average length of the interconnect are increasing. Furthermore, high-speed operation in high-density circuits can cause unanticipated signal problems. In order to design high-density and high-speed VLSI circuits, accurate knowledge of the electrical characteristics of the interconnect is essential [1]–[6]. Then signal delay, transient, and crosstalk problems can be avoided.

The conventional RC interconnect circuit model is based on simplifying assumptions that are inaccurate at high frequencies. The model accounts only for capacitive coupling, assumes interconnect line parameters are constant with frequency, neglects dielectric loss, and restricts circuit loading conditions. Many methods that predict exact interconnect circuit response have been constructed [2], [6]–[9]. The coupled interconnect line transfer functions under unmatched, but special case terminal conditions have been reported in many paper [3], [7]–[10]. However, these interconnect signal simulations are not accurate for submicron VLSI-based high-speed circuits because some assumptions were made that are the same as those of the RC models.

A new expression for the n-coupled interconnect system transfer function has been derived under general linear generator and uncoupled load conditions, i.e., without any restrictions in circuit load impedance or circuit generator impedance. Under these generalized conditions, high-speed signals on coupled interconnects have been simulated. In this simulation, generalized interconnect circuit parameters (all line parameters are frequency dependent) have been used. The line parameter models are based on high-frequency s-parameter measurements [11]. The validity of the interconnect model parameters was verified in previous work [11] with low-frequency and s-parameter measurement techniques. Interconnect simulations using the generalized interconnect transfer function has been verified with time-domain measurements using an HP54121T high-speed sampling oscilloscope. The simulations and measurements show good agreement.

For practical interconnect circuit simulation, it is virtually impossible to consider all high-frequency-related effects such as frequency dependence of the line parameters, substrate coupling effects, 3-D effects, nonlinear loading effects, etc., at one time. This paper's contribution is a theoretical analysis of n-coupled line interconnect with frequency-variant line parameters. A high-speed experimental measurement of on-chip IC interconnect coupled line response demonstrates the accuracy of the analysis. Moreover, the generalized transfer function in this analysis lends itself to using experimental data as input. Thus, an engineer can use the generalized transfer function and the results in [11] to generate comparisons between existing interconnect circuit simulation models and high-frequency s-parameter measurement-based modeling and simulation.

The general guidelines for interconnect circuit modeling are under continual revision with increasing IC transistor performance and continual reduction in IC interconnect linewidth and spacing. There exists a difficult tradeoff among interconnect model accuracy, complexity, and efficiency. This theoretical analysis can be used to evaluate the accuracy of simplified interconnect circuit models for high-speed circuit simulation by providing accurate estimates of signal delay, jitter, and crosstalk.

II. n-Coupled Line Interconnect Transfer Function

To perform transient simulations of coupled interconnect circuits, it is necessary to have an accurate circuit transfer function. This section develops a new circuit transfer function for multiconductor coupled interconnects with frequency-dependent parameters. The load impedance, linear generator impedance, and number of lines is unrestricted.

Manuscript received July 26, 1993; revised September 14, 1994. This work was supported by the Semiconductor Research Corporation under Contract 92-SP-087.

Y. Eo is with the Department of Electrical Engineering, Hanyang University, Ansan, Kyung-Do, Korea.

W. R. Eisenstadt is with the VLSI TCAD Group, Department of Electrical Engineering, University of Florida, Gainesville, FL 32611 USA.

IEEE Log Number 9410336.

Electrical properties of multiconductor transmission lines can be simulated by the following matrix form representation of the Telegrapher's equations:

$$\frac{d[V(x)]}{dx} = [Z_s][I(x)] \tag{1}$$

$$\frac{d[I(x)]}{dx} = [Y_p][V(x)] \tag{2}$$

where $[V(x)]$ and $[I(x)]$ are line voltages and currents and $[Z_s]$ and $[Y_p]$ are composed of

$$[Z_s] = [R] + j\omega[L] = \begin{bmatrix} Z_{11} & \cdots & Z_{1n} \\ \vdots & \ddots & \vdots \\ Z_{n1} & \cdots & Z_{nn} \end{bmatrix} \tag{3}$$

$$[Y_p] = [G] + j\omega[C] = \begin{bmatrix} Y_{11} & \cdots & Y_{1n} \\ \vdots & \ddots & \vdots \\ Y_{n1} & \cdots & Y_{nn} \end{bmatrix} \tag{4}$$

where

$$C_{ii} = \sum_{j=1}^{n} c_{ij} \quad \text{and} \quad C_{ij} = -c_{ij}; \tag{5}$$

similarly,

$$G_{ii} = \sum_{j=1}^{n} g_{ij} \quad \text{and} \quad G_{ij} = -g_{ij}. \tag{6}$$

The propagation constant and characteristic impedance are derived by solving eigenvalue equations. The voltage eigenmatrix $[S_v]$ and current eigenmatrix $[S_i]$ are the solutions of the eigenvalue equations

$$(\gamma^2[U] - [Z_S][Y_P])[S_v] = 0 \tag{7}$$

$$[S_i] = [Z_S]^{-1}[S_v][\Lambda] \tag{8}$$

where $[U]$ is the identity matrix and $[\Lambda]$ is the diagonal matrix, diag $\{\gamma_1, \gamma_2, \cdots, \gamma_n\}$. Note that the square roots of the eigenvalues are physical propagation constants.

Solving the eigenvalue equation (7) with boundary conditions of Fig. 1, the following matrix equation can be derived (9), shown at the bottom of the page, where the coupled line voltage eigenmatrix $[S_v]$ and current eigenmatrix $[S_i]$ can be readily determined and $[E(x)]$ is a diagonal matrix,

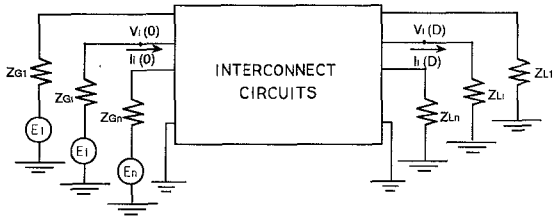

Fig. 1. Multiconductor interconnect circuits with arbitrary generator impedances and load impedances.

diag $\{e^{-\gamma_1 x}, \cdots, e^{-\gamma_n x}\}$. Also, $[C_1]$ and $[C_2]$ are matrices of voltage wave magnitudes. Thus, $[C_1]$ represents port voltage magnitudes for propagation in the reverse direction, and $[C_2]$ represents port voltage magnitudes for propagation in the forward direction. In (9), the system matrix can be uniquely determined if the following are known: 1) voltage eigenmatrix and current eigenmatrix, 2) input and output impedances, and 3) propagation constant matrix and characteristic impedance matrix which require knowledge of transmission line parameter matrices $[R]$, $[L]$, $[C]$, and $[G]$. Among these, 3) is the most important because it physically represents the particular interconnect system characteristics. Quantities 1) and 2) can be readily determined from a given interconnect system configuration.

Representing (9) in a simpler linear matrix form

$$[b] = [A][X] \tag{10}$$

where (see (11), shown at the bottom of the page)

$$[X] = \begin{bmatrix} [C_1] \\ [C_2] \end{bmatrix} = \begin{bmatrix} x_1 \\ \vdots \\ x_n \\ x_{n+1} \\ \vdots \\ x_{2n} \end{bmatrix} \tag{12}$$

$$[b] = \begin{bmatrix} [E_i] \\ [0] \end{bmatrix} \tag{13}$$

where

$$[E_i] = \begin{bmatrix} 0 \\ \vdots \\ E_i \\ \vdots \\ 0 \end{bmatrix}. \tag{14}$$

$$\begin{bmatrix} [E_i] \\ [0] \end{bmatrix} = \begin{bmatrix} [S_v] + [Z_G][S_i] & [S_v] - [Z_L][S_i] \\ ([S_v] + [Z_L][S_i])[E(D)] & ([S_v] - [Z_L][S_i])[E(D)]^{-1} \end{bmatrix} \begin{bmatrix} [C_1] \\ [C_2] \end{bmatrix} \tag{9}$$

$$[A] = \begin{bmatrix} a_{11} & \cdots & a_{12n} \\ \vdots & \ddots & \vdots \\ a_{2n1} & \cdots & a_{2n2n} \end{bmatrix} = \begin{bmatrix} [S_v] + [Z_G][S_i] & [S_v] - [Z_L][S_i] \\ ([S_v] + [Z_L][S_i])[E(D)] & ([S_v] - [Z_L][S_i])[E(D)]^{-1} \end{bmatrix} \tag{11}$$

Now, a new matrix $[B^j]$ is defined as a matrix in which the jth column of matrix $[A]$ is replaced by the column matrix $[b]$, i.e.

$$[B^j] = \begin{bmatrix} a_{11} & \cdots & a_{1j-1} & 0 & a_{1j+1} & \cdots & a_{12n} \\ & & & \vdots & & & \\ \vdots & \ddots & \vdots & E_i & \vdots & \ddots & \vdots \\ a_{2n1} & \cdots & a_{2nj-1} & 0 & a_{2nj+1} & \cdots & a_{2n2n}. \\ & & & & & & \end{bmatrix} \tag{15}$$

Thus, solving (10) with Cramer's rule yields the components of the port wave magnitudes of the system

$$x_j = \frac{E_i \Delta_{ij}}{\det(A)} \tag{16}$$

where

$$\Delta_{ij} = \mathrm{Cof}_{ij}(B^j). \tag{17}$$

Since input signals (voltages) at the n-coupled interconnects are

$$\begin{aligned}[V] &= [S_v]\left(\begin{bmatrix} x_1 \\ \vdots \\ x_n \end{bmatrix} + \begin{bmatrix} x_{n+1} \\ \vdots \\ x_{2n} \end{bmatrix}\right) \\ &= [S_v]([C_1] + [C_2]), \end{aligned} \tag{18a}$$

the response of n-coupled interconnect is rewritten as

$$\begin{aligned}[V] &= \begin{bmatrix} s_{11} & \cdots & s_{1n} \\ \vdots & \ddots & \vdots \\ s_{n1} & \cdots & s_{nn} \end{bmatrix}\left(\begin{bmatrix} x_1 \\ \vdots \\ x_n \end{bmatrix} + \begin{bmatrix} x_{n+1} \\ \vdots \\ x_{2n} \end{bmatrix}\right) \\ &\triangleq \left(\begin{bmatrix} p_1 \\ \vdots \\ p_n \end{bmatrix} + \begin{bmatrix} q_1 \\ \vdots \\ q_n \end{bmatrix}\right) = \begin{bmatrix} p_1 + q_1 \\ \vdots \\ p_n + q_n \end{bmatrix} \end{aligned} \tag{18b}$$

where

$$\begin{cases} p_i = \sum_{j=1}^{n} s_{ij} x_j \\ q_i = \sum_{j=1}^{n} s_{ij} x_{n+j}. \end{cases} \tag{19}$$

Thus

$$\begin{aligned} V_i &= p_i + q_i \\ &= \sum_{j=1}^{n} s_{ij}(x_j + x_{n+j}). \end{aligned} \tag{20}$$

To determine overall interconnect system response, the superposition principle is applied. Consider each independent source as follows. If E_1 is excited and other sources are zero, that is, if

$$E_1 \neq 0 \quad \text{and} \quad E_2 = E_3 = \cdots = E_n = 0,$$

then the following circuit responses can be determined:

$$\left(\frac{V_1}{E_1}, \frac{V_2}{E_1}, \cdots, \frac{V_n}{E_1}\right). \tag{21a}$$

If E_2 is excited and other sources are zero, that is, if

$$E_2 \neq 0 \quad \text{and} \quad E_1 = E_3 = \cdots = E_n = 0,$$

then the following circuit responses can be determined:

$$\left(\frac{V_1}{E_2}, \frac{V_2}{E_2}, \cdots, \frac{V_n}{E_2}\right). \tag{21b}$$

Similarly, extending these procedures on the nth source E_n, that is, if

$$E_n \neq 0 \quad \text{and} \quad E_1 = E_2 = \cdots = E_{n-1} = 0,$$

then all circuit responses can be determined

$$\left(\frac{V_1}{E_n}, \frac{V_2}{E_n}, \cdots, \frac{V_n}{E_n}\right). \tag{21c}$$

From (21) and the superposition principle, transfer functions of each line are determined. That is, the transfer function of line 1 is

$$\begin{aligned} H_1 &= \frac{V_1}{E_1} + \frac{V_1}{E_2} + \cdots + \frac{V_1}{E_n} \\ &= V_1 \sum_{i=1}^{n}\left(\frac{1}{E_i}\right), \end{aligned} \tag{22a}$$

the transfer function of line 2 is

$$\begin{aligned} H_2 &= \frac{V_2}{E_1} + \frac{V_2}{E_2} + \cdots + \frac{V_2}{E_n} \\ &= V_2 \sum_{i=1}^{n}\left(\frac{1}{E_i}\right), \end{aligned} \tag{22b}$$

and similarly, the transfer function of line n is

$$\begin{aligned} H_n &= \frac{V_n}{E_1} + \frac{V_n}{E_2} + \cdots + \frac{V_n}{E_n} \\ &= V_n \sum_{i=1}^{n}\left(\frac{1}{E_i}\right). \end{aligned} \tag{22c}$$

Thus, the generalized interconnect transfer function of line j for a given n-conductor system is

$$\begin{aligned} H_j &= V_j \sum_{i=1}^{n}\left(\frac{1}{E_i}\right) \\ &= \left[\sum_{k=1}^{n} s_{jk}(x_k + x_{n+k})\right]\left[\sum_{i=1}^{n}\frac{1}{E_i}\right]. \end{aligned} \tag{23}$$

In (23), s_{jk} is a component of voltage eigenmatrix $[S_v]$ and x_k and x_{n+k} can be determined from (16). Note that (23) cannot be simply determined; thus, a computer program or symbolic software analysis package such as Mathematica or Maple can aid in this calculation.

III. Generalized Transfer Function of Two Coupled Lines

Reducing the matrix equation (9) with eigenmatrices and boundary conditions for two coupled lines, the transfer functions of two coupled lines in the frequency domain including frequency-dependent line parameters and linear uncoupled loading conditions, i.e., $Z_{G1} \neq Z_{G2} \neq Z_{L1} \neq Z_{L2}$, can be determined. The matrix of constants $[C_1]$ of two coupled lines in (9) is the magnitude of incident waves at the launching ports determined from boundary conditions

$$[C_1] = \begin{bmatrix} V_1^+(x=0) \\ V_2^+(x=0) \end{bmatrix}. \tag{24}$$

Similarly, the matrix of constants $[C_2]$ of two coupled lines is the magnitude of reflected waves at the launching ports determined from boundary conditions. Thus

$$[C_2] = \begin{bmatrix} V_1^-(x=0) \\ V_2^-(x=0) \end{bmatrix}. \tag{25}$$

Combining (9), (24), and (25), the two line transfer functions are given by

$$H_1(\omega) = \frac{1}{\det(A(\omega))}\{T_1(\omega) + T_2(\omega)\} \tag{26}$$

$$H_2(\omega) = \frac{1}{\det(A(\omega))}\{T_1(\omega) - T_2(\omega)\} \tag{27}$$

where H_1 and H_2 are transfer functions on line 1 (active line) and line 2 (quiet line), respectively, and

$$T_1(\omega) = \{\mathrm{Cof}_{11}(A(\omega))\exp(-\gamma_1(\omega)x) + \mathrm{Cof}_{13}(A(\omega))\exp(\gamma_1(\omega)x)\} \tag{28}$$

$$T_2(\omega) = \{\mathrm{Cof}_{12}(A(\omega))\exp(-\gamma_2(\omega)x) + \mathrm{Cof}_{14}(A(\omega))\exp(\gamma_2(\omega)x)\} \tag{29}$$

where $\mathrm{Cof}_{ij}(A)$ is the cofactor of square matrix $[A]$ which is given by

$$[A(\omega)] \equiv \begin{bmatrix} A_1(\omega) \\ A_2(\omega) \\ A_3(\omega) \\ A_4(\omega) \end{bmatrix} \tag{30}$$

where the respective row vectors of matrix $[A]$ are given by

$$[A_1(\omega)] = \left(\left(\frac{Z_1(\omega)+Z_{G1}}{Z_1(\omega)}\right) \left(\frac{Z_2(\omega)+Z_{G1}}{Z_2(\omega)}\right) \left(\frac{Z_1(\omega)-Z_{G1}}{Z_1(\omega)}\right) \left(\frac{Z_2(\omega)-Z_{G1}}{Z_2(\omega)}\right)\right)$$

$$[A_2(\omega)] = \left(\left(\frac{Z_1(\omega)+Z_{G2}}{Z_1(\omega)}\right) -\left(\frac{Z_2(\omega)+Z_{G2}}{Z_2(\omega)}\right) \left(\frac{Z_1(\omega)-Z_{G2}}{Z_1(\omega)}\right) -\left(\frac{Z_2(\omega)-Z_{G2}}{Z_2(\omega)}\right)\right)$$

$$[A_3(\omega)] = \left(\left(\frac{Z_1(\omega)-Z_{L1}}{Z_1(\omega)}\right)\exp(-\gamma_1(\omega)l) \left(\frac{Z_2(\omega)-Z_{L1}}{Z_2(\omega)}\right)\exp(-\gamma_2(\omega)l) \left(\frac{Z_1(\omega)+Z_{L1}}{Z_1(\omega)}\right)\exp(\gamma_1(\omega)l) \left(\frac{Z_2(\omega)+Z_{L1}}{Z_2(\omega)}\right)\exp(\gamma_2(\omega)l)\right)$$

$$[A_4(\omega)] = \left(\left(\frac{Z_1(\omega)-Z_{L2}}{Z_1(\omega)}\right)\exp(-\gamma_1(\omega)l) -\left(\frac{Z_2(\omega)-Z_{L2}}{Z_2(\omega)}\right)\exp(-\gamma_2(\omega)l) \left(\frac{Z_1(\omega)+Z_{L2}}{Z_1(\omega)}\right)\exp(\gamma_1(\omega)l) -\left(\frac{Z_2(\omega)+Z_{L2}}{Z_2(\omega)}\right)\exp(\gamma_2(\omega)l)\right).$$

Solving the eigenvalue equation (7) in a two-line coupled system, the propagation constants of the lines are given by

$$\gamma_1 = \sqrt{(Y_{11}+Y_{12})(Z_{11}+Z_{12})} \tag{31}$$

$$\gamma_2 = \sqrt{(Y_{11}-Y_{12})(Z_{11}-Z_{12})} \tag{32}$$

where γ_1 and γ_2 are propagation constants of the eigenmodes. Similarly, the characteristic impedance matrix is defined as the ratio of the incident voltage wave to the reflected voltage wave. The characteristic impedance can be represented in terms of voltage eigenmatrix and current eigenmatrix as follows:

$$[Z] = [S_v][S_i]^{-1}. \tag{33}$$

Thus, the characteristic impedance matrix of two coupled lines is given by

$$[Z] = \frac{1}{2}\begin{bmatrix} Z_1+Z_2 & Z_1-Z_2 \\ Z_1-Z_2 & Z_1+Z_2 \end{bmatrix} \tag{34}$$

where

$$Z_1 = \sqrt{\frac{Z_{11}+Z_{12}}{Y_{11}+Y_{12}}} \quad \text{and} \quad Z_2 = \sqrt{\frac{Z_{11}-Z_{12}}{Y_{11}-Y_{12}}}. \tag{35}$$

Note that both the propagation constant and characteristic impedance matrices have been represented by the series impedance matrix of (3) and parallel admittance matrix of (4).

If $Z_{G1} = Z_{G2}$ and $Z_{L1} = Z_{L2}$ are assumed and the frequency-dependent components are replaced by constant parameters, this equation reduces to formulas in the literature [7], [8]

$$H_1 = \frac{1}{2}(T_1 + T_2) \tag{36}$$

$$H_2 = \frac{1}{2}(T_1 - T_2) \tag{37}$$

where

$$T_1 = \frac{Z_1}{Z_1 + Z_G} \frac{\exp(-\gamma_1 x) + \rho_{L1} \exp(-\gamma_1(2l - x))}{1 - \rho_{G1}\rho_{L1} \exp(-2\gamma_1 l)}$$

$$T_2 = \frac{Z_2}{Z_2 + Z_G} \frac{\exp(-\gamma_2 x) + \rho_{L2} \exp(-\gamma_2(2l - x))}{1 - \rho_{G2}\rho_{L2} \exp(-2\gamma_2 l)}$$

where

$$\rho_{L1} = \frac{Z_L - Z_1}{Z_L + Z_1}, \qquad \rho_{G1} = \frac{Z_G - Z_1}{Z_G + Z_1},$$

$$\rho_{L2} = \frac{Z_L - Z_2}{Z_L + Z_2}, \quad \text{and} \quad \rho_{G2} = \frac{Z_G - Z_2}{Z_G + Z_2}.$$

With further assumptions, (36) and (37) can be represented in closed form in the time domain. Moreover, if impedance matching conditions are satisfied, then an even simpler form is produced [12]

$$H_i = \exp(-\gamma_i x). \tag{38}$$

This simplified form of the interconnect transfer function has been widely used in many applications at low frequencies or in carefully designed microwave circuits with matched generator and load resistances [12]–[14].

IV. Simulation Algorithm

Given this generalized multiconductor interconnect transfer function in the frequency domain, a method of time-domain simulation needed to be developed. For an input pulse function which is excited in IC interconnect, a very stable method of pulse decomposition was employed [15]. Using this pulse decomposition method, the pulse rise time and fall time can be approximated as the summation of delayed unit step functions. The input function is

$$f(t) = \sum_{i=1}^{n} f_i(t) \tag{39}$$

where

$$f_i(t) = \frac{A}{n}\left[U\left(t - \left(\frac{i-1}{n}\right)t_r\right) \cdot -U\left(t - \left(\frac{i-1}{n}\right)t_r - t_f\right)\right]. \tag{40}$$

Given the interconnect line circuit parameter matrices, the time-domain responses of the interconnect under generalized conditions can be obtained by inverse Fourier transform of (40)

$$V_i(t, x) = \mathcal{F}^{-1}[F_i(\omega)H_i(\omega, x)] \tag{41}$$

where i is the line number and x is the distance.

This generalized multiconductor transfer function and Fourier transform technique were used for simulation. A new algorithm (software) was developed for the simulations, and the simulations were verified with picosecond pulsed measurements of interconnect lines described in Section V. Using the generalized interconnect transfer function requires knowledge of the multiconductor interconnect line circuit parameter matrices $[R]$, $[L]$, $[C]$, and $[G]$ and terminal conditions of interconnect circuits $[Z_G]$ and $[Z_L]$.

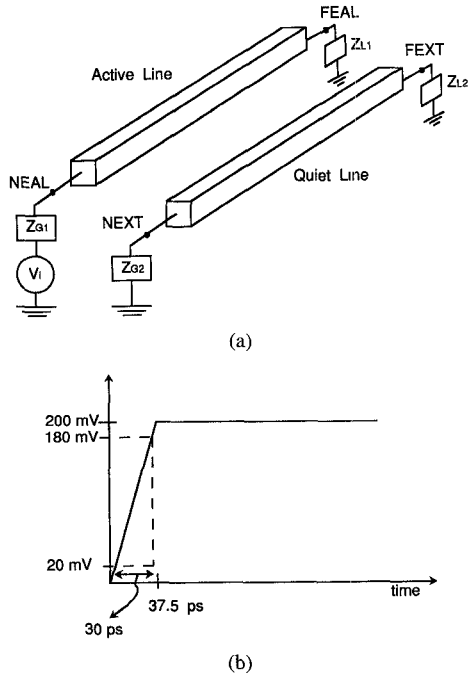

Fig. 2. (a) Two coupled interconnect circuit test points. (b) Input waveform of unit step pulse.

The frequency-dependent properties of the single conductor and coupled interconnect circuit models are reported [11], [16]. These model parameters are broken into three generic components. These are on-diagonal interconnect parameters (self-parameters), coupling capacitance parameters, and coupling inductance parameters. The on-diagonal parameters of the line circuit parameter matrix are calculated from the single-line interconnect frequency-dependent model [11]. The coupling capacitance can be calculated by PISCES-IIB simulation [17] or analytical models [18]–[20]. Then, the coupling inductance is found via the free space capacitance matrix [16].

V. Simulation and Experimental Verification in the Time Domain

In an example of an coupled interconnect circuit, the signal test points are $V_1(t, 0)$, $V_2(t, 0)$, $V_1(t, l)$, and $V_2(t, l)$, as shown in Fig. 2. The acronyms used in Fig. 2 are, in order, signal at the near end of the activated line (NEAL), the near-end crosstalk (NEXT), signal at the far-end activated line (FEAL), and the far-end crosstalk (FEXT). These are the signal nodes in the interconnect circuit simulations. Fig. 3 shows test structure layouts and cross section.

Time-domain simulation shows signal transients, propagation, and crosstalk at the four coupled interconnect circuit test nodes with termination impedances as defined in Fig. 2. Given an input signal applied at V_i, signal transients can be observed in the four test points. Propagation delay and signal degradation can be observed in the test point FEAL. The NEXT and FEXT show crosstalk at the quiet line.

The coupled interconnect circuit simulations employ the generalized interconnect transfer function, i.e., (26) and (27),

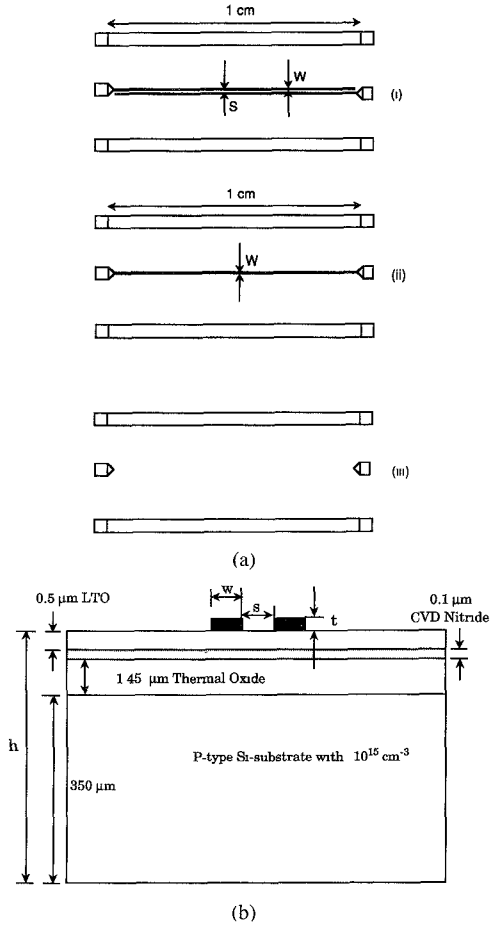

Fig. 3. (a) Cross-coupled interconnect test structure layout. (i) Cross-coupled test structure. (ii) Single line test structure. (iii) Open test structure. (b) Test structure cross-section.

and the frequency-dependent interconnect circuit parameter model (frequency-dependent RLCG model) [16]. These circuit simulations are verified using picosecond time-domain measurements.

The line spacing of the cross-coupled lines is 2 μm and the line width is 4 μm. They are fabricated over an SiO_2 layer, a thin-film nitride layer, and a p-type Si-substrate with the concentration of 10^{15} cm^{-3}. For the time-domain measurements, an HP54121T sampling oscilloscope is connected to the Cascade Microtech Probe Station and the DUT is mounted on the measurement chuck. The termination condition of the measurement system is 50 Ω at the measurement points.

Two-port network measurements make it possible to observe the FEXT from a cross-coupled test structure. Thus, if floating terminals of the DUT are assumed to have very high resistance (1 MΩ), then the simulation is easily done. Since the internally generated input function of the HP54121T sampling oscilloscope is a unit step with a 30 ps rise time [21], measurement results can be compared with the simulation results under the same conditions. As expected from simulation, the signal is delayed and dispersed, and there is crosstalk noise due to coupling.

Fig. 4(a) shows simulated reflected signal transients for near-end and far-end crosstalk of a quiet time (FEXT). Fig. 4(b) shows time-domain measurements of the reflected

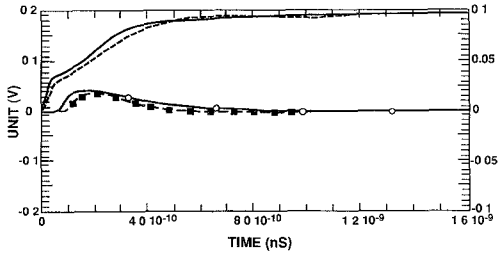

Fig. 4. Simulation and measurements of 4-μm linewidth and 2-μm line-spacing coupled-line response. Simulated reflected signal at NEAL (solid lines) and transmitted signal at FEXT (solid lines with circles). Measured reflection signal of the above coupled lines at NEAL (dashed lines) and transmitted signal at FEXT (dashed lines with boxes).

signal transients and crosstalk for the far end of the quiet line (FEXT). Similar results were obtained for all measured and simulated test points [16].

The simulation employed the frequency-variant RLCG model for diagonal element determination of transmission line circuit parameter matrices [11]. The comparison of the simulated and experimental results shows good agreement with experimental data. The narrow IC interconnect (4 and 2 μm) showed good agreement with measured data in magnitude, delay, and waveform. Wider IC interconnect (10 μm) show good agreement in waveform and delay, but substantial magnitude error. The narrow interconnect is typically encountered in VLSI circuits. Sources of error include the simplified parameter extraction methodology, time-domain measurement error, and the pad parasitic response model.

This work shows that experimental measurements of interconnect signal transmission can be accurately estimated by the new generalized interconnect transfer function, that is, signal transient, crosstalk noise, and delay, which are essential information for IC circuit designs, can be predicted. The interconnect simulation can, with minor modifications, include high-frequency parasitic effects. These effects are hard to independently observe using existing time-domain experimental tools.

VI. Summary and Discussion

Through an exact mathematical analysis, the generalized interconnect transfer function for coupled lines is derived. Using frequency-dependent parameter modeling of coupled interconnect, high-speed VLSI interconnect simulations have been performed. To verify these theoretical analyses, computer simulation and experiments in the time domain have been performed.

Test structures with cross-coupled lines were designed, and time-domain measurements were performed with a high-speed sampling oscilloscope, HP54121T. The experimental results showed good agreement with simulation results.

Today's high-speed circuit design faces very difficult and challenging modeling problems. Unlike low-frequency circuit designs, there are many sources of interconnect crosstalk (IC substrate coupling, capacitive coupling, inductive coupling, and package-related coupling) and three-dimensional parasitic effects. These are difficult to verify by simulation or experimental techniques. Indeed, the authors feel that char-

acterizing all performance aspects of the multilevel-metal network of signal transmission lines in high-speed VLSI circuits requires excessive computer resources or experimental resources. Models used for industrial design of VLSI circuits in SPICE or in VLSI timing simulators are highly simplified by necessity. There needs to be extensive experimental verification and determination of interconnect model error for high-performance digital circuit design. The error range of existing interconnect models can be investigated by comparing existing interconnect modeling with simulations based on the generalized interconnect transfer function. In addition, designers will need to use circuit simulation techniques such as SPICE and microwave circuit simulators on critical circuit paths in their circuit designs. The results in this paper can be used to simulate critical paths and subcircuits in IC designs.

REFERENCES

[1] M. Hatamian, L. A. Hornak, T. E. Little, S. K. Tewksbury, and P. Franzon, "Fundamental interconnect issues," *AT&T Tech. J.*, vol. 66, pp. 13–30, July 1987.

[2] D. Winklestein, M. B. Steer, and R. Pomerleau, "Simulation of arbitrary transmission line networks with nonlinear terminations," *IEEE Trans. Circuits Syst.*, vol. 38, pp. 418–422, Apr. 1991.

[3] J. E. Schutt-Aine and R. Mittra, "Nonlinear transient analysis of coupled transmission lines," *IEEE Trans. Circuits Syst.*, vol. 36, pp. 959–966, July 1989.

[4] A. Deutsch, G. V. Kopcsay, V. A. Ranieri, J. K. Cataldo, E. A. Galligan, W. S. Graham, R. P. McGouey, S. L. Nunes, J. R. Paraszczak, J. J. Ritsko, R. J. Serino, D. Y. Shih, and J. S. Wilczynsik, "High-speed signal propagation on lossy transmission lines," *IBM J. Res. Develop.*, vol. 34, pp. 601–615, July 1990.

[5] K. W. Goosen and R. B. Hamond, "Modeling of picosecond pulse propagation in microstrip interconnections on integrated circuits," *IEEE Trans. Microwave Theory Tech.*, vol. 37, pp. 469–478, Mar. 1989.

[6] J. C. Liao, O. A. Plansinski, and J. L. Prince, "Computation of transients in lossy VLSI packaging interconnections," *IEEE Trans. Components, Hybrids, Manufact. Technol.*, vol. 13, pp. 833–838, Dec. 1990.

[7] H. You and M. Soma, "Crosstalk analysis of interconnect lines and packages in high speed integrated circuits," *IEEE Trans. Circuits Syst.*, vol. 37, pp. 1019–1026, Aug. 1990.

[8] L. T. Hwang, D. Nayak, I. Turlik, and A. Reisman, "Thin-film pulse propagation analysis using frequency techniques," *IEEE Trans. Components, Hybrids, Manufact. Technol.*, vol. 14, pp. 192–198, Mar. 1991.

[9] G. Ghione, I. Maio, and G. Vecchi, "Modeling of multiconductor buses and analysis of crosstalk, propagation delay and pulse distortion in high-speed GaAs logic circuits," *IEEE Trans. Microwave Theory Tech.*, vol. 37, pp. 445–456, Mar. 1989.

[10] J. C. Isaacs, Jr. and N. A. Strakhov, "Crosstalk in uniformly coupled lossy transmission line," *Bell Syst. Tech. J.*, vol. 52, pp. 101–115, Jan. 1973.

[11] Y. Eo and W. R. Eisenstadt, "High speed VLSI interconnect modeling based on S-parameter measurements," *IEEE Trans. Components, Hybrids, Manufact. Technol.*, pp. 555–562, Aug. 1993.

[12] R. L. Veghte and C. A. Balanis, "Dispersion of transient signals in microstrip transmission lines," *IEEE Trans. Microwave Theory Tech.*, vol. MTT-34, pp. 1427–1436, Dec. 1986.

[13] J. F. Whitaker, T. B. Norris, G. Mourou, and T. Y. Hsiang, "Pulse dispersion and shaping in microstrip lines," *IEEE Trans. Microwave Theory Tech.*, vol. MTT-35, pp. 41–47, Jan. 1987.

[14] H. Curtins and A. V. Shah, "Pulse behavior of transmission lines with dielectric losses," *IEEE Trans. Circuits Syst.*, vol. CAS-32, pp. 819–826, Aug. 1985.

[15] Y. Ikawa, W. R. Eisenstadt, and R. W. Dutton, "Modeling of high-speed, large-signal transistor switching transients from S-parameter measurements," *IEEE Trans. Electron Dev.*, vol. ED-29, pp. 669–675, Apr. 1982.

[16] Y. Eo, "Microwave-measurement-based IC interconnect characterization, modeling, and simulation for high speed VLSI circuit design," Ph.D. dissertation, Univ. Florida, Gainesville, May 1993.

[17] "TMA PISCES-IIB, Two-dimensional device analysis program," version 9033, Technology Modeling Associates Inc., Palo Alto, CA, Nov. 15, 1990.

[18] T. Sakurai and K. Tamaru, "Simple formula for two- and three-dimensional capacitances," *IEEE Trans. Electron Dev.*, vol. ED-30, pp. 183–185, Feb. 1983.

[19] C. P. Yuan, "Modeling and extraction of interconnect parameters in VLSI circuits," Ph.D. dissertation, Univ. Illinois, Urbana–Champaign, 1983.

[20] J.-H. Chern, J. Huang, L. Arledge, P.-C. Li, and P. Yang, "Multilevel metal capacitance model for CAD design synthesis systems," *IEEE Electron Dev. Lett.*, vol. 13, pp. 32–34, Jan. 1992.

[21] HP 54121T Digitizing Oscilloscope, Hewlett Packard Co., Santa Rosa, CA, 1990.

Yungseon Eo received the B.S. and M.S. degrees in electronic engineering from Hanyang University, Seoul, Korea, in 1983 and 1985, respectively, and the Ph.D. degree in electrical engineering from the University of Florida, Gainesville, in 1993. During his Ph.D. program, he performed research in the area of IC interconnect characterization, modeling, and simulation for high-speed VLSI circuit design.

From 1986–1988, he worked at Korea Telecommunication Authority Research Center, Seoul, where he performed telecommunication network planning and software design. From 1993–1994, he performed s-parameter-based BJT device characterization and modeling for high-speed circuit design at Applied Micro Circuits Corporation, San Diego, CA. In 1994, he worked in the Research and Development Center of LSI Logic, Santa Clara, CA. He is currently working as an assistant professor at Hanyang University, Ansan, Kyungki-Do, Korea. His research interest is in high-frequency measurements and high-performance VLSI circuit design.

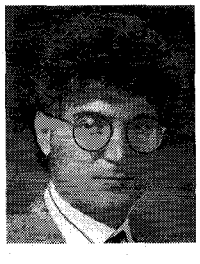

William R. Eisenstadt received the B.S., M.S., and Ph.D. degrees in electrical engineering from Stanford University, Stanford, CA, in 1979, 1981, and 1986, respectively.

In 1984, he joined the faculty of the University of Florida, Gainesville, where he is now an associate professor. His research is concerned with high-frequency characterization, simulation and modeling of integrated circuit devices, packages, and interconnect. In addition, he is interested in large-signal microwave circuit and analog circuit design.

Dr. Eisenstadt received the NSF Presidential Young Investigator Award in 1985.